



Human *CIDE*C transgene improves lipid metabolism and protects against high-fat diet–induced glucose intolerance in mice

Received for publication, January 14, 2022, and in revised form, July 8, 2022 Published, Papers in Press, August 11, 2022,

<https://doi.org/10.1016/j.jbc.2022.102347>

Abhishek Gupta¹, Bijinu Balakrishnan¹, Shakun Karki², Mark Slayton¹ , Sukanta Jash³, Sayani Banerjee³, Tan Hooi Min Grahn⁴, Srikanthika Jambunathan⁵, Sarah Disney¹, Hebaallaha Hussein¹, Dong Kong⁶, Bradford B. Lowell^{7,8}, Purushothaman Natarajan⁹ , Umesh K. Reddy⁹ , Noyan Gokce², Vishva M. Sharma^{1,*}, and Vishwajeet Puri^{1,*}

From the ¹Department of Biomedical Sciences and Diabetes Institute, Heritage College of Osteopathic Medicine, Ohio University, Athens, Ohio, USA; ²Evans Department of Medicine and Whitaker Cardiovascular Institute, Boston University School of Medicine, Boston, Massachusetts, USA; ³Alpert Medical School of Brown University, Brown University, Providence, Rhode Island, USA; ⁴Division of Molecular Medicine and Gene Therapy, Lund Stem Cell Center, Lund University Hospital, Lund, Sweden; ⁵Department of Medicine, Boston University School of Medicine, Boston, Massachusetts, USA; ⁶Division of Endocrinology, Department of Pediatrics, F.M. Kirby Neurobiology Center, Boston Children's Hospital and Harvard Medical School, Boston, Massachusetts, USA; ⁷Division of Endocrinology, Diabetes, and Metabolism, Department of Medicine, Beth Israel Deaconess Medical Center, Boston, Massachusetts, USA; ⁸Program in Neuroscience, Harvard Medical School, Boston, Massachusetts, USA; and ⁹Department of Biology, West Virginia State University, Institute, West Virginia, USA

Edited by Dennis Voelker

Cell death–inducing DNA fragmentation factor-like effector C (*CIDE*C) expression in adipose tissue positively correlates with insulin sensitivity in obese humans. Further, E186X, a single-nucleotide *CIDE*C variant is associated with lipodystrophy, hypertriglyceridemia, and insulin resistance. To establish the unknown mechanistic link between *CIDE*C and maintenance of systemic glucose homeostasis, we generated transgenic mouse models expressing *CIDE*C (Ad-*CIDE*Ctg) and *CIDE*C E186X variant (Ad-*CIDE*Cmut) transgene specifically in the adipose tissue. We found that Ad-*CIDE*Ctg but not Ad-*CIDE*Cmut mice were protected against high-fat diet–induced glucose intolerance. Furthermore, we revealed the role of *CIDE*C in lipid metabolism using transcriptomics and lipidomics. Serum triglycerides, cholesterol, and low-density lipoproteins were lower in high-fat diet–fed Ad-*CIDE*Ctg mice compared to their littermate controls. Mechanistically, we demonstrated that *CIDE*C regulates the enzymatic activity of adipose triglyceride lipase *via* interacting with its activator, CGI-58, to reduce free fatty acid release and lipotoxicity. In addition, we confirmed that *CIDE*C is indeed a vital regulator of lipolysis in adipose tissue of obese humans, and treatment with recombinant *CIDE*C decreased triglyceride breakdown in visceral human adipose tissue. Our study unravels a central pathway whereby adipocyte-specific *CIDE*C plays a pivotal role in regulating adipose lipid metabolism and whole-body glucose homeostasis. In summary, our findings identify human *CIDE*C as a potential ‘drug’ or a ‘druggable’ target to reverse obesity–induced lipotoxicity and glucose intolerance.

Adipose tissue is a major regulator of metabolic health (1). Obesity is a significant health problem (1, 2), which broadly refers to excess adipose tissue. It is accompanied by increases in type 2 diabetes and cardiometabolic disease, the conditions linked to insulin resistance and glucose intolerance (1, 3). One of the main pathological causes is chronically elevated circulating free fatty acids (FFAs) and triglycerides (TGs) due to impaired adipose lipid homeostasis (1, 4). The identification of new therapeutic avenues aimed at maintaining lipid homeostasis and glucose tolerance is crucial to meet the need for the treatment of obesity and associated comorbidities.

Lipolysis of TGs stored in adipose tissue releases fatty acids (FAs) under conditions of metabolic need. Lipolysis of TGs to FFAs and glycerol requires three consecutive steps that involve three different enzymes: adipose triglyceride lipase (ATGL; also called desnutrin and PNPLA2), hormone-sensitive lipase (HSL), and monoacylglycerol lipase (MGL). ATGL is the rate-limiting enzyme for lipolysis in adipocytes and catalyzes the first step of hydrolysis of triglycerides to diacylglycerol (5–8). CGI-58, a potent stimulator of ATGL catalytic activity, triggers ATGL-mediated lipolysis under physiologically stimulating conditions (9). In the basal state, perilipin A (PLIN1) prevents CGI-58 access to ATGL, restricting lipolysis (7, 9–11). Under basal conditions, ATGL is primarily localized in endoplasmic reticulum–related membranes in the cytoplasm and is in complex with its inhibitor, G0/G1 switch gene 2, GOS2 (12). Upon β -adrenergic stimulation, PKA activation results in PLIN1 phosphorylation at multiple sites, causing the release of CGI-58, which then binds and stimulates ATGL (10, 13). Translocation of unbound ATGL to lipid droplets, along with phosphorylated HSL, leads to acute activation of triglyceride hydrolysis.

* For correspondence: Vishva M. Sharma, sharmav@ohio.edu; Vishwajeet Puri, puri@ohio.edu.

CIDEA improves glucose homeostasis and whole-body metabolism

Prolonged β -adrenergic stimulation downregulates G0S2 and releases additional ATGL for sustained lipolysis.

Cell death-inducing DNA fragmentation factor-like effector (CIDE)-protein family members, CIDEA and CIDEA (also known as FSP27), play an important role in regulating fat metabolism in adipocytes (14–17). CIDEA is an abundantly expressed lipid droplet-associated protein in adipocytes, where it regulates fat storage and release (14, 16). CIDEA expression is low in patients with insulin resistance and obesity (15), and weight loss surgery improves insulin sensitivity while increasing CIDEA expression (18). Further, a nonsense mutation (E186X) in CIDEA causes lipodystrophy, dyslipidemia, and insulin-resistant type 2 diabetes (19). *In vitro*, CIDEA appears to regulate ATGL-mediated lipolysis (16) or represses ATGL transcription (20). While these reports show a positive association between CIDEA and insulin sensitivity in humans, none showed a direct effect of CIDEA in maintaining systemic glucose homeostasis.

Although mouse and human CIDEA isoforms differ in their cellular and physiological effects, especially with regard to insulin signaling and glucose homeostasis (15, 16, 19, 21–23), all studies in humans, both *in vitro* and *in vivo*, unequivocally show a positive association of CIDEA with healthy metabolic phenotypes (15, 16, 18, 19, 24–31). The present study establishes a direct link between human CIDEA and the maintenance of systemic lipid and glucose homeostasis. To investigate the adipose-specific role of human CIDEA and determine its mechanism of action, we generated two innovative transgenic mouse models expressing either full-length or mutant human CIDEA (E186X) in adipose tissue. We performed clinical human and experimental animal model investigations to identify a novel mechanism of CIDEA-mediated regulation of the lipolysis to protect against high-fat diet (HFD)-induced glucose intolerance.

Results

CIDEA expression negatively associates with increased lipolysis in visceral adipose tissue of patients with obesity

Obese human subjects undergoing planned bariatric surgery were recruited for the study; each provided paired subcutaneous adipose tissue (SAT) and visceral adipose tissue (VAT) samples at baseline, which were partitioned for different experiments. Table 1 shows the clinical characteristics of all participants. Glycerol release, a measure of lipolysis, was assessed in adipose tissue samples isolated during bariatric surgery. As expected (32), higher lipolysis was observed in VAT compared to SAT (Fig. 1A). Given this ~2.5-fold difference, we measured the expression of lipases ATGL and HSL, which catalyze the breakdown of TGs. Unexpectedly, gene and protein expression of ATGL and HSL revealed no significant difference between VAT and SAT depots (Fig. 1, B–E). This was surprising because ATGL and HSL are major enzymes for lipolysis in adipocytes (33), with ATGL as the first and rate-limiting enzyme in TG hydrolysis (8, 9, 34). Because our previous studies showed that CIDEA regulates ATGL-mediated lipolysis in primary human adipocytes (16) and

Table 1
Clinical characteristics of obese human subjects

Parameter	Obese (n=52)
Age (years)	41 ± 14
Female (%)	87.3
BMI (kg/m ²)	44.1 ± 7
Waist circumference (cm)	123 ± 7
Weight (kg)	120 ± 18
Insulin (mIU/ml)	17.1 ± 14
Glucose (mg/dl)	111 ± 49
HbA1C (%)	6.1 ± 1.9
HOMA-IR	6.5 ± 8.5
hsCRP (mg/dl)	9.0 ± 7.6
Triglycerides (mg/dl)	121 ± 60
Total cholesterol (mg/dl)	177 ± 48
HDL-C (mg/dl)	43.1 ± 10
LDL-C (mg/dl)	110 ± 37
Systolic BP (mmHg)	131.1 ± 14
Diastolic BP (mmHg)	74.5 ± 12
Diabetes mellitus (%)	35
Hypertension (%)	40
Hypercholesterolemia (%)	43

Data are mean ± SD.
BP, blood pressure.

CIDEA positively correlates with reduced circulatory FFAs and insulin sensitivity in people with obesity (15, 30), we examined the expression of CIDEA in the paired VAT and SAT samples. Accumulation of visceral fat has been more closely and clinically linked to metabolic dysfunction, and we determined that CIDEA expression was significantly lower in VAT compared to SAT (Fig. 1, F and G).

Generation and characterization of adipose-specific CIDEA transgenic mice

To investigate the underlying molecular mechanism(s) of CIDEA-regulated adipose lipolysis and its effect on whole-body metabolism, we generated a transgenic mouse model expressing human CIDEA without altering endogenous mouse *Cidec* expression (Fig. 2A). To generate transgenic animals, a floxed stop codon followed by the human CIDEA expression cassette was inserted into the mouse *Rosa26* locus. To generate mice expressing human CIDEA in adipose tissue depots (Ad-CIDEAtg), floxed mice were bred with B6.FVB-Tg (Adipoq-cre)1Evdrl/J mice from Jackson Laboratory that express Cre recombinase enzyme under the control of mouse adiponectin promoter/enhancer regions (Fig. 2A). Specific primer pairs for human CIDEA and Cre recombinase were used to confirm the presence of either transgene (see Experimental procedures) (Fig. 2B). Mice expressing only human CIDEA were used as floxed controls, whereas mice expressing both human CIDEA and Cre, termed Ad-CIDEAtg, were used as experimental models. To validate the adipose-specific expression of CIDEA, we performed quantitative RT-PCR and analyzed relative gene expression levels in various organs of Ad-CIDEAtg mice. Quantitative RT-PCR results confirmed that CIDEA was expressed in adipose depots only (*i.e.*, perigonadal, inguinal, and brown adipose depots) (Fig. 2C). CIDEA protein expression was assessed using Western blot analysis in insulin-sensitive organs. The antibody could not distinguish between human and mouse isoforms of CIDEA, so we expected increased expression of CIDEA in

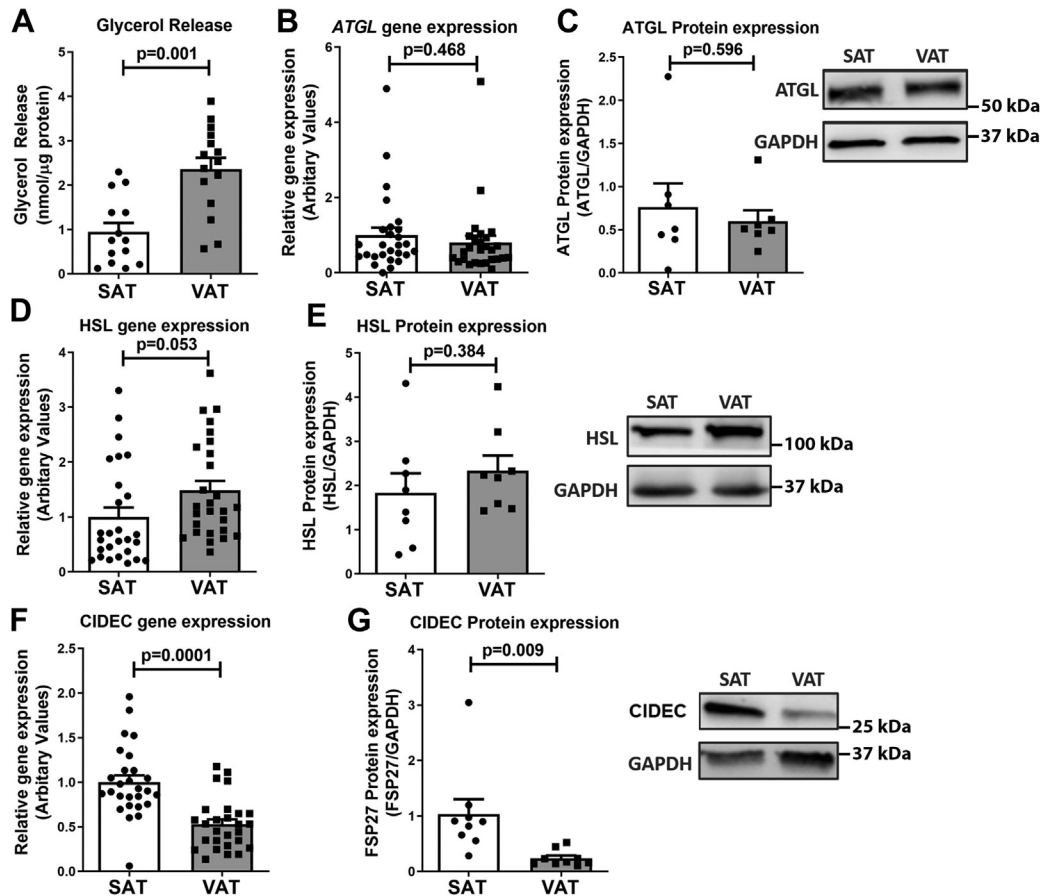


Figure 1. CIDEc expression negatively associates with lipolysis in the adipose tissue of patients with obesity. A, basal lipolysis, assessed as glycerol release, was measured in 12 SAT and 15 VAT depots of human patients and normalized to total protein. Data are presented as mean \pm SEM. B, basal ATGL mRNA in paired SAT and VAT depots of 27 human study participants. Data are presented as mean \pm SEM. C, ATGL protein expression in SAT and VAT paired samples from eight randomly selected patients, with obesity among the 27 samples. Data are presented as mean \pm SEM. D, basal HSL mRNA in paired SAT and VAT depots of 27 human participants. Data are presented as mean \pm SEM. E, HSL protein expression in SAT and VAT paired samples from eight randomly selected patients with obesity. F, CIDEc mRNA in 27 paired SAT and VAT depots of patients with obesity. Data are presented as mean \pm SEM. G, CIDEc protein level measured in paired SAT and VAT depots of eight randomly selected patients. Data are presented as mean \pm SEM. For statistical significance, unpaired *t* test was used to analyze the significance between two groups. SAT, subcutaneous adipose tissue; VAT, visceral adipose tissue.

adipose tissue depots. Indeed, there was higher expression of total CIDEc protein (approximately 3-fold increase) in adipose depots (Fig. 2D).

Metabolic characterization of Ad-CIDEcTg mice

Ad-CIDEcTg and floxed-littermate control mice were fed regular chow or HFD (60% kcal from fat) beginning at 3 months of age. Metabolic phenotyping was performed after 10 weeks of regular chow or HFD feeding. Body weight assessment indicated an almost equal increase in weight among transgenic and control mice (Fig. S1A). The slightly higher weight gain in Ad-CIDEcTg mice was not statistically significant. White adipose tissue, brown adipose tissue, and liver collected after the completion of the metabolic study also did not significantly differ in weight between the same diet groups (Fig. S1B). Differences in food intake (Fig. S1C) and energy intake were not significant between floxed and Ad-CIDEcTg mice fed a similar diet (Fig. S1D) nor was fat or lean mass normalized to body weight (Fig. S1, E and F). There was no significant difference in oxygen consumption, carbon

dioxide exhalation, respiratory exchange ratio, energy expenditure, or ambulatory activity between Ad-CIDEcTg mice and their littermate floxed controls (Fig. S1, G and H and S2).

Ad-CIDEcTg mice were protected against HFD-induced glucose intolerance

We next evaluated the effect of HFD on glucose homeostasis in Ad-CIDEcTg and their floxed-littermate controls. Ad-CIDEcTg mice showed significantly higher glucose tolerance in an i.p. glucose tolerance test (GTT) compared to floxed-control mice fed HFD (Fig. 3A). Insulin (0.75 IU/kg) was injected i.p. in fasted mice. Consistent with GTT, Ad-CIDEcTg mice exhibited improved insulin tolerance (Fig. 3B). Thus, Ad-CIDEcTg mice were protected against HFD-induced glucose intolerance and insulin resistance. Measurement of fasting blood glucose revealed a significant reduction in glucose levels in Ad-CIDEcTg mice fed HFD (Fig. 3C), indicating improved glucose homeostasis in Ad-CIDEcTg mice. Serum leptin levels exhibited a decreasing trend, whereas serum adiponectin was unchanged in HFD-fed

CIDEC improves glucose homeostasis and whole-body metabolism

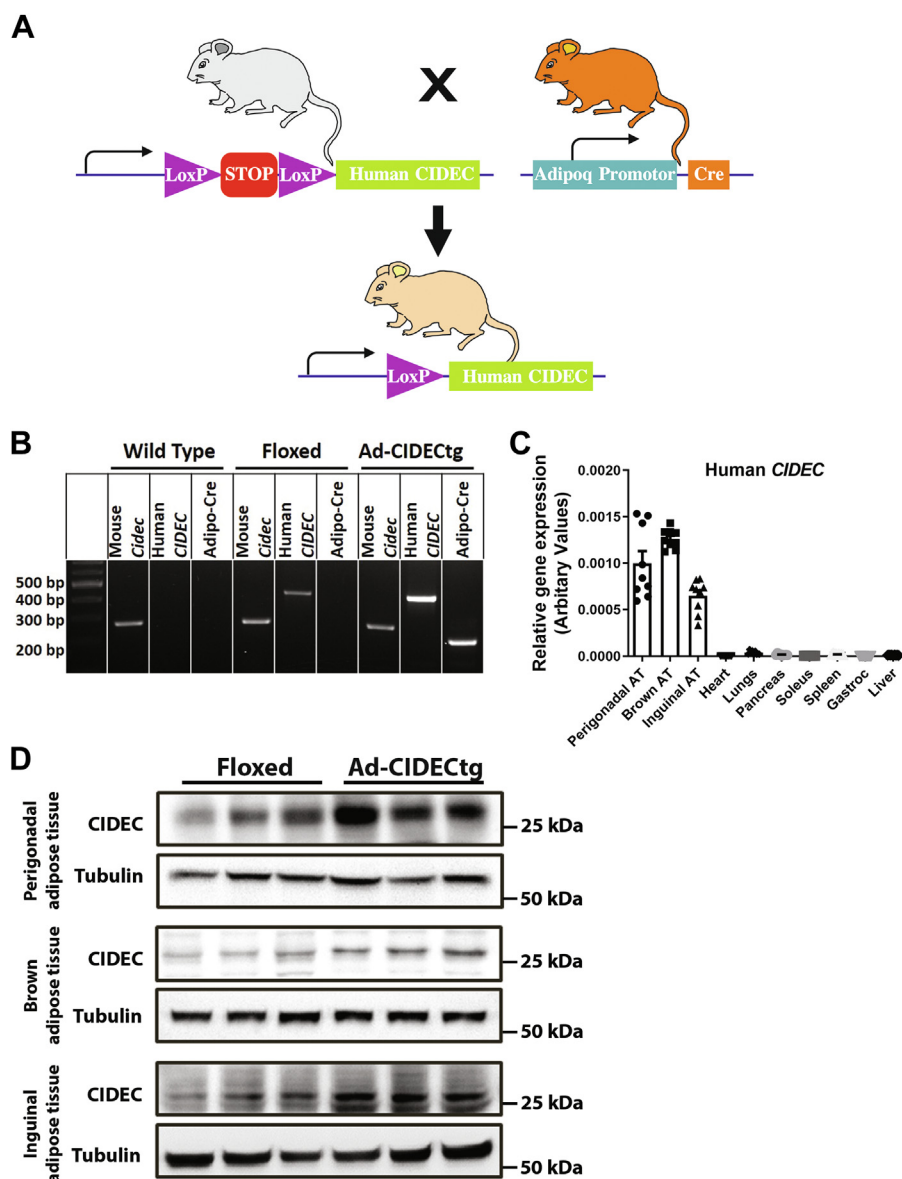


Figure 2. Generation and characterization of Ad-CIDECtg transgenic mice expressing human CIDEC specifically in adipose tissue. *A*, schematic representation of the generation of Ad-CIDECtg mice expressing *CIDEC* in adipose tissue. *B*, genotyping of mice to assess the presence of human CIDEC and/or Cre recombinase. *C*, relative gene expression of human *CIDEC* in different organs of Ad-CIDECtg mice ($n = 3$ per group). *D*, protein expression of CIDEC in different adipose tissue depots including perigonadal white adipose tissue, inguinal adipose tissue (subcutaneous adipose tissue), and interscapular adipose tissue (brown adipose tissue) of male floxed and male Ad-CIDECtg mice ($n = 3$ per group).

Ad-CIDECtg mice (Fig. 3, *D* and *E*). The leptin/adiponectin ratio, which positively correlates with type 2 diabetes (35), exhibited a decreasing trend in HFD-fed Ad-CIDECtg mice (Fig. 3*F*). Finally, to assess the effect of adipose tissue-specific expression of human CIDEC on organ-specific insulin sensitivity, mice were injected with insulin (i.p.) and measured AKT phosphorylation. AKT is a nodal protein in the insulin signaling pathway and a measure of insulin signaling in perigonadal adipose tissue, liver, and skeletal muscle. Ad-CIDECtg mice, when fed HFD, showed improved AKT phosphorylation in perigonadal adipose tissue and skeletal muscle, suggestive of improved systemic insulin sensitivity (Fig. 3, *G* and *H*). Also, we measured insulin levels before and after glucose injection in HFD-fed floxed-controls and Ad-

CIDECtg mice. As expected, HFD-fed Ad-CIDECtg mice had slightly lower basal insulin levels compared to HFD-fed floxed-control mice. After the glucose injection, the control group showed higher levels of circulating insulin compared to transgenic mice at 2 min and 5 min time points. However, the significance could not be achieved due to the high level of variability in the insulin levels of floxed-controls compared to the Ad-CIDECtg mice. Subsequent time points showed comparable levels of circulating insulin in both groups. These data suggest that the pancreas is normal in both the groups and Ad-CIDECtg mice are more insulin sensitive when fed a HFD (Fig. S3). Overall, these results led us to conclude that adipose-specific expression of CIDEC regulates whole-body glucose homeostasis and insulin sensitivity.

CIDEC improves glucose homeostasis and whole-body metabolism

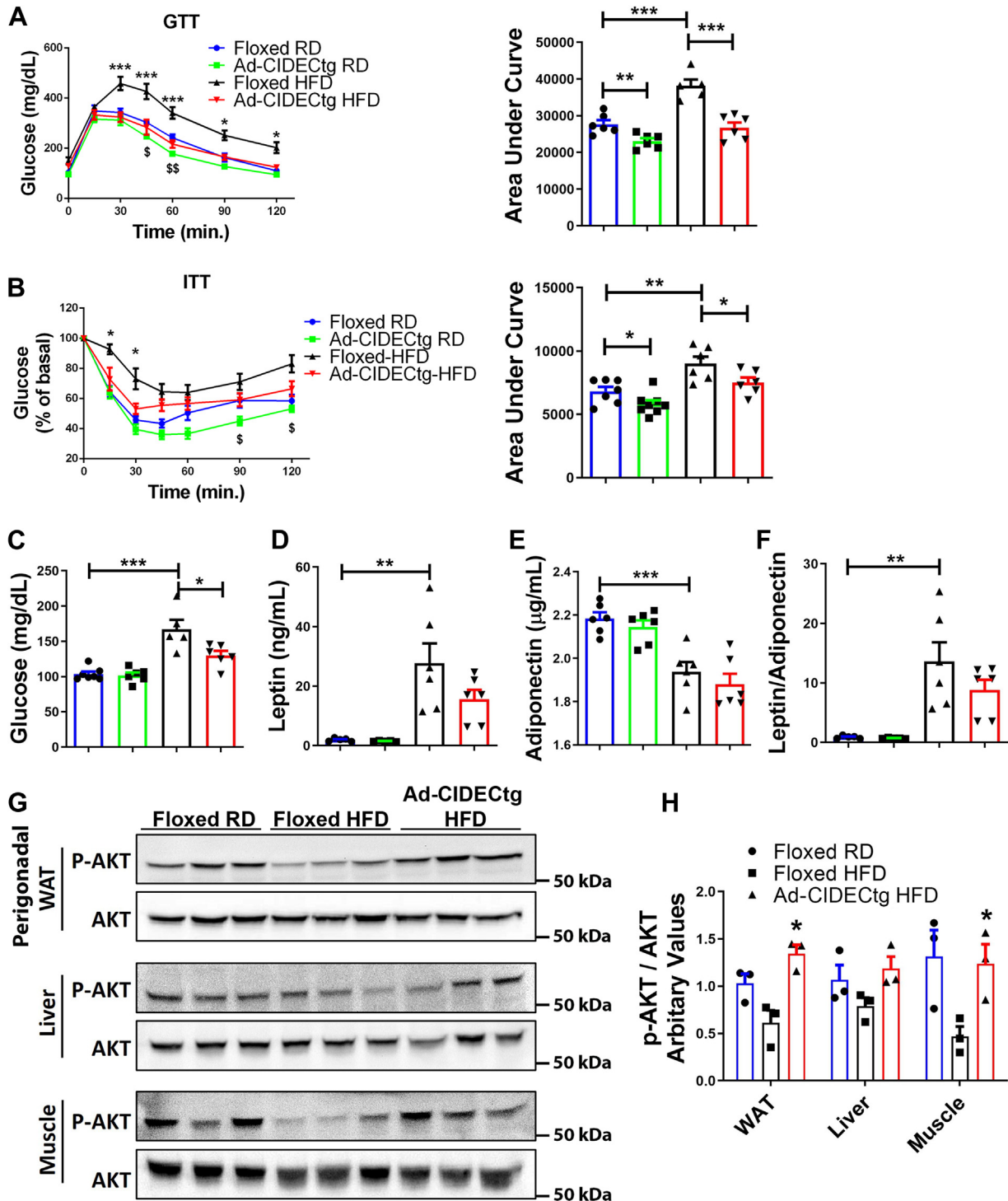


Figure 3. Ad-CIDECtg mice exhibit protection against high fat diet (HFD)-induced glucose intolerance. *A*, i.p. GTT in 4.5 month old (3 months + 1.5 months HFD) male floxed or Ad-CIDECtg mice either on a regular diet (RD) or HFD for 10 weeks. The plot on the right-hand side represents area under the curve (AUC). * signifies statistical significance between the HFD-fed groups, and ^s signifies statistical significance between the RD-fed groups. *B*, ITT of floxed or Ad-CIDECtg mice either on a RD or HFD. The plot on the right-hand side represents the AUC. * signifies statistical significance between the HFD-fed groups, and ^s signifies statistical significance between the RD-fed groups. *C*, fasting blood glucose levels in mice. *D*, serum leptin levels, (*E*) serum adiponectin levels, and (*F*) leptin/adiponectin ratio. In *C–F*, blue, green, black, and red bars represent floxed RD, Ad-CIDECtg RD, floxed HFD, and Ad-CIDECtg HFD, respectively. *G*, Western blot analysis representing relative insulin-stimulated AKT phosphorylation (Ser473) levels in insulin-sensitive tissues including white adipose tissue, liver, and muscle (gastrocnemius), and (*H*) densitometry analysis of Western blots. Data are represented as mean \pm SEM. For statistical analysis, two-way ANOVA followed by Bonferroni post hoc analysis was performed for (*A*) and (*B*). For other graphs, a student's *t* test was applied to compare the significance between the two groups. **p* < 0.05, ***p* < 0.01, ****p* < 0.001 and ^s*p* < 0.05, ^{ss}*p* < 0.01, ^{sss}*p* < 0.001 (n = 6–8 per group). GTT, glucose tolerance test.

CIDEC improves glucose homeostasis and whole-body metabolism

Transcriptome analysis of Ad-CIDEC^{Tg} mice adipose tissue revealed improved lipid metabolism

To identify changes in gene expression and metabolic pathways triggered by adipose tissue expression of human CIDEC in Ad-CIDEC^{Tg} mice, we performed RNA-seq analysis in adipose tissue paired with pathway enrichment analysis. Differentially expressed genes (DEGs) between floxed and Ad-CIDEC^{Tg} mice were identified using the EdgeR tool. After filtering by $p < 0.05$ (false discovery rate) and $\text{Log}_2\text{FoldChange} > 1$, we detected 1431 DEGs. Among these, 670 were downregulated and 761 were upregulated. Pathway analysis of these DEGs revealed 26 upregulated pathways (Fig. 4A) and 12 downregulated pathways (Fig. 4B). Interestingly, many upregulated genes were associated with lipid metabolism pathways. A volcano plot depicting upregulated (red), downregulated (blue), and unaltered (gray) DEGs is displayed in Figure 4C. Interestingly, most of the upregulated genes in adipose tissue of Ad-CIDEC^{Tg} mice were associated

with lipid homeostasis. The heat map in Figure 4D shows altered genes associated with lipid metabolism in Ad-CIDEC mice. Overall, our transcriptome analysis aligned with previous studies suggesting the role of CIDEC in lipid homeostasis (31).

Serum lipid parameters and FFA species were reduced in Ad-CIDEC^{Tg} mice

We hypothesized that serum lipid parameters would be reduced in Ad-CIDEC^{Tg} mice. Indeed, serum TG levels were significantly lower in HFD-fed Ad-CIDEC^{Tg} mice (Fig. 5A). Total cholesterol (Fig. 5B) and low-density lipoprotein (LDL) levels (Fig. 5C) were also significantly reduced in HFD-fed Ad-CIDEC^{Tg} mice. Levels of high-density lipoproteins (HDLs) in Ad-CIDEC^{Tg} mice exhibited an increasing trend (Fig. 5D). Total nonesterified FAs were significantly lower in HFD-fed Ad-CIDEC^{Tg} mice compared to littermate-floxed controls (Fig. 5E). To get a deeper insight into the FFA species, we

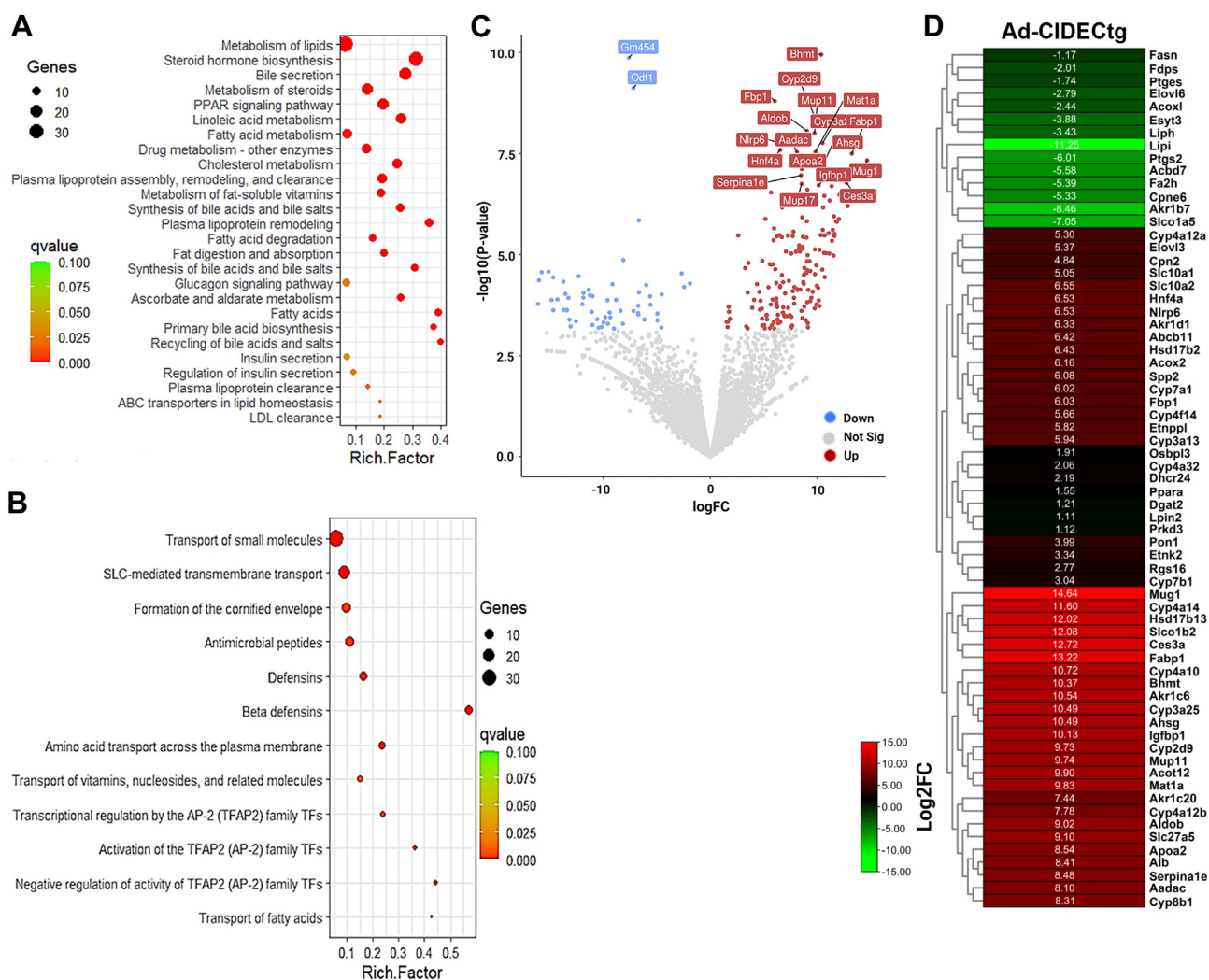


Figure 4. RNA-seq analysis in white adipose tissue of floxed and Ad-CIDEC^{Tg} mice. **A**, significantly enriched (q value < 0.05) biological pathways among upregulated DEGs, and **(B)** downregulated pathways in adipose tissue of Ad-CIDEC^{Tg} mice. The rich factor is the ratio of the number of DEGs to the total gene number in a pathway. Here, the q -value is a corrected p -value. The color and size of the dots represent the range of q -value and the number of DEGs mapped to the indicated pathways, respectively. **C**, volcano plot representing differentially expressed genes in floxed versus Ad-CIDEC^{Tg} mice. **D**, heat map showing altered genes associated with lipid metabolism in perigonadal adipose tissue of Ad-CIDEC^{Tg} mice. DEG, differentially expressed gene.

CIDEc improves glucose homeostasis and whole-body metabolism

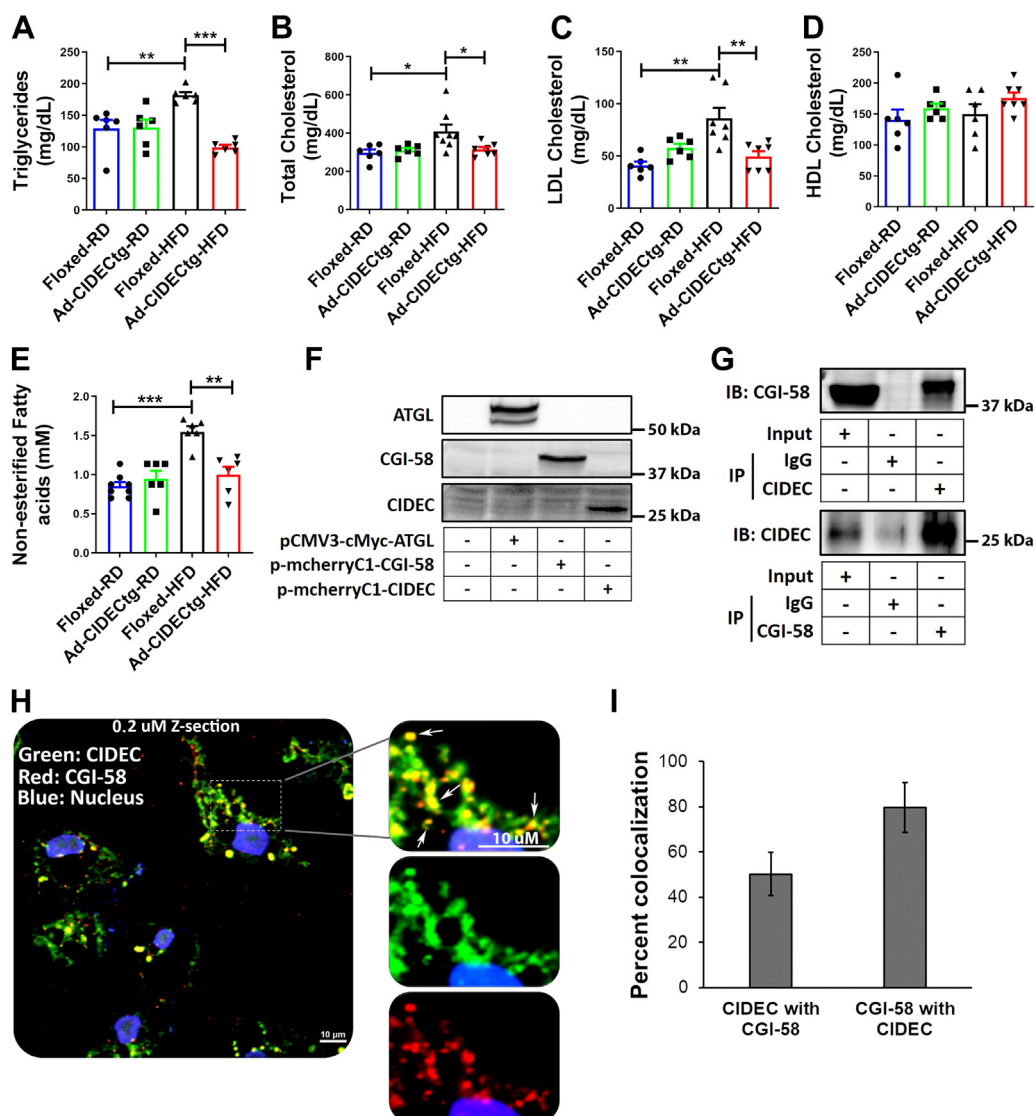


Figure 5. CIDEc interacts with CGI-58. Fasting serum lipid parameters were analyzed in floxed and Ad-CIDEcTg mice fed regular chow or HFD. *A*, serum triglycerides, *B*) serum total cholesterol, *C*) low-density lipoprotein, *D*) high-density lipoprotein, and *E*) nonesterified fatty acids. *F*, Western blot analysis to confirm the overexpression of human ATGL, human CGI-58, and human CIDEc. *G*, immunoprecipitation of human CIDEc from cell lysates of human CIDEc and human CGI-58 overexpressing HEK-293 cells and immunoblotting against CGI-58 antibody (top panel). Immunoprecipitation of CGI-58 from cell lysates of human CIDEc and human CGI-58 overexpressing HEK-293 cells and immunoblotting against CIDEc (lower panel). *H*, a Z-slice of 0.2 μm showing localization of CIDEc (green) and CGI-58 (red) in culture human adipocytes. Yellow color shows colocalization of CIDEc and CGI-58. *I*, semiquantitative analysis of CIDEc colocalized to CGI-58 (green to red), and CGI-58 colocalized to CIDEc (red to green) (n = 10). HFD, high-fat diet.

performed lipidomics on serum samples from Ad-CIDEcTg and floxed littermates, which showed a significant reduction in various FA species in serum FFA, cholesterol, and TG fractions in Ad-CIDEcTg mice (Table S1). Next, we assessed adipocyte morphology and size in the perigonadal adipose tissue of floxed-controls and Ad-CIDEcTg mice. Although the adipocyte size appeared slightly bigger in the Ad-CIDEcTg mice, no significant change was observed in adipocyte number (Fig. S4). Overall, these results supported the role of CIDEc in improved lipid homeostasis.

CIDEc interacts with CGI-58 and limits ATGL activation

Our previous *in vitro* study showed that CIDEc suppresses ATGL-mediated lipolysis in cultured adipocytes (16).

However, the molecular action of CIDEc-mediated suppression of ATGL-mediated lipolysis is not yet known. No change in ATGL and HSL expression was observed in the adipose tissue of obese human subjects (Fig. 1); we therefore hypothesized that CIDEc might regulate FFA release *via* its action on ATGL catalytic activity. Since CGI-58 is a potent activator of ATGL, we tested whether CIDEc regulates ATGL activity *via* CGI-58. We used coimmunoprecipitation to investigate CIDEc and CGI-58 interaction. First, we overexpressed human-CGI-58, human-ATGL, and human-CIDEc in HEK293 cells and confirmed their expression by Western blot (Fig. 5F). Immunoprecipitation with CIDEc and immunoblotting against CGI-58 confirmed that CIDEc and CGI-58 interact (Fig. 5G top panel). Inversely, immunoprecipitation with CGI-58 and immunoblotting against CIDEc confirmed

CIDEc improves glucose homeostasis and whole-body metabolism

CGI-mediated pull down of CIDEc (Fig. 5G bottom panel). Next, we sought to determine the distribution of CIDEc and CGI-58 in cultured human adipocytes. Confocal microscopy on cells immunolabeled with CIDEc and CGI-58 antibodies revealed significant colocalization of CGI-58 and CIDEc (Fig. 5H). Semiquantitative measurement showed over 80% CGI-58 was colocalized with CIDEc in cultured human adipocytes (Fig. 5J).

To test our hypothesis that CGI-58-mediated stimulation of ATGL activity is impaired by CIDEc, ATGL catalytic activity was performed in the presence of ATGL, CGI-58, and CIDEc, either individually or in combination. ATGL or CGI-58 alone had a modest increase in lipolysis compared to controls; however, ATGL-mediated lipolysis was significantly enhanced by CGI-58 (Fig. 6A). Interestingly, adding CIDEc did not affect lipolysis in the presence of ATGL alone, but it significantly reduced lipolysis induced by the combination of ATGL and CGI-58 (Fig. 6A), indicating that CGI-58 action on ATGL was inhibited by CIDEc. To further confirm the effect of CIDEc on CGI-58 action, we used recombinant CIDEc protein (rCIDEc) and performed a lipase activity assay. rCIDEc significantly reduced the effect of CGI-58 on the catalytic activity of ATGL (Fig. 6A).

To confirm the role of human CIDEc transgene in adipose tissue lipolysis *in vivo*, we measured basal and stimulated lipolysis in isolated mouse white adipose tissue from Ad-CIDEctg mice and the littermate controls. Adipose tissue explants were incubated with or without CL-316,243 (2 μ M) for 2 h, and glycerol release was measured. Under both basal and stimulated conditions, adipose tissue from Ad-CIDEctg mice showed significantly reduced glycerol release (Fig. 6B), thus confirming the role of adipose-specific expression of CIDEc in decreasing lipolysis. Furthermore, to assess the role of CIDEc in lipolysis in human adipose tissue, we used loss- and gain-of-function experiments using CIDEc siRNA and rCIDEc, to deplete or overexpress CIDEc, respectively, in human adipose tissue explants. Interestingly, siRNA-mediated CIDEc depletion in SAT increased lipolysis (Fig. 6C), whereas treatment of human VAT with rCIDEc significantly decreased lipolysis (Fig. 6D).

Transgenic mice expressing mutant human-CIDEc were not protected from HFD-induced insulin resistance

Finally, to confirm the consequential role of human CIDEc in FA homeostasis and protection against HFD-induced

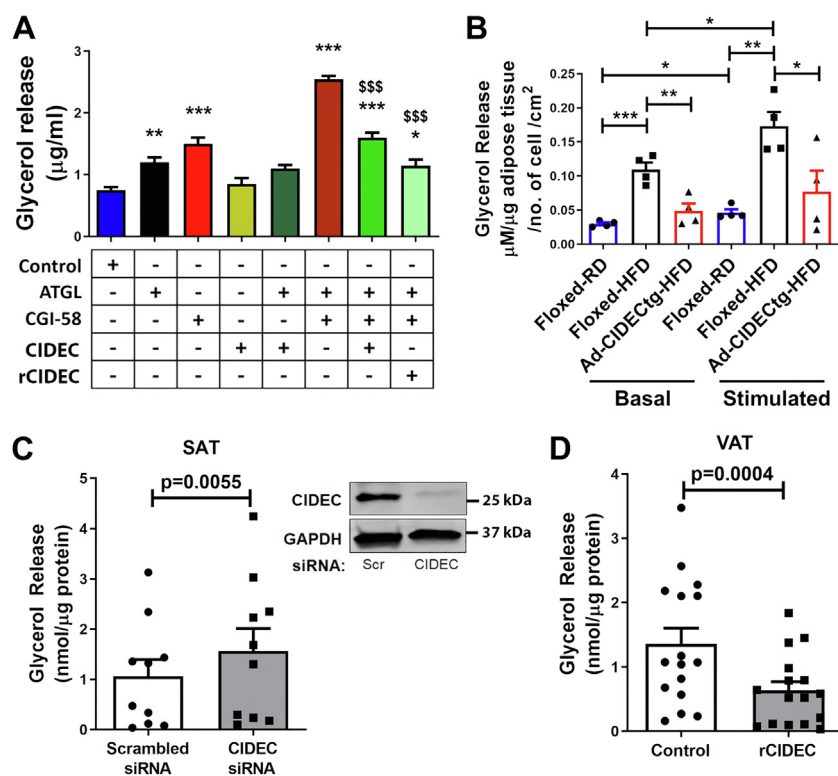


Figure 6. CIDEc limits CGI-58-induced ATGL activation to release FFAs. A, measurement of glycerol lipolysis upon addition of cell lysates overexpressing either ATGL, CGI-58, or CIDEc alone or in different combinations to assess ATGL-induced lipolytic activity. * signifies statistical significance compared to controls, [§] signifies statistical significance compared to the lipolysis measured in column 6 (ATGL+CGI-58). One-way ANOVA was performed to analyze the significance between multiple groups (n = 3 per group). *p < 0.05, **p < 0.01, ***p < 0.001 and [§]p < 0.05, ^{§§}p < 0.01, ^{§§§}p < 0.001. B, glycerol release was assessed in *ex vivo* explants of white adipose tissue of mice either unstimulated or stimulation with CL-316243 (2 μ M) for 2 h. Data are represented as mean \pm SEM. For statistical analyses, a student's t test was applied to compare two groups. *p < 0.05, **p < 0.01, ***p < 0.001. C, glycerol release was assessed in the adipose tissue from SAT depot (n = 10) after siRNA-mediated CIDEc knockdown. Scrambled siRNA was used as a control. Top right panel is a representative Western blot showing siRNA-mediated CIDEc knockdown in SAT. D, glycerol release from the VAT depot (n = 16) after 24 h of control (DMSO) and recombinant CIDEc (rCIDEc) treatment. Data are presented as mean \pm SEM. Paired t test was performed to analyze the significance between the two groups. DMSO, dimethyl sulfoxide; FFA, free fatty acid; SAT, subcutaneous adipose tissue; VAT, visceral adipose tissue.

insulin resistance, we generated an innovative adipose tissue-specific mouse model expressing human *CIDEA* (556G→T) mutation, Ad-CIDEA_{mut}. A known single nucleotide polymorphism in *CIDEA* produces a nonfunctional protein causing partial lipodystrophy, hypertriglyceridemia, and insulin-resistant type 2 diabetes (19). The transversion mutation of guanine to thymine at complementary DNA (cDNA) nucleotide position 556 in exon 6 of *CIDEA* results in a premature stop codon (19). Since *CIDEA* was suggested to undergo homodimeric or heterodimeric functional interactions (36, 37), we hypothesized that a mouse model expressing the *CIDEA* (556G→T) variant might show a dominant-negative effect of *CIDEA* on metabolic parameters. The floxed Ad-CIDEA_{mut} mouse model was generated in the same manner as the human *CIDEA* full-length in Figure 2. Sequencing results confirmed the presence of this mutation in Ad-CIDEA_{mut} mice (Fig. 7A). Crossing Ad-CIDEA_{mut} floxed mice with mice expressing Cre recombinase under adiponectin promoter expressed the *CIDEA* mutant variant in the adipose tissue (Fig. 7B). Ad-CIDEA_{mut} and floxed-littermate control mice were fed either regular chow or HFD for 10 weeks beginning at 3 months of age. No change in weight gain was observed between the regular chow or HFD groups (Fig. 7C). Weight of perigonadal adipose tissue, brown adipose tissue, and liver was unaltered between groups (Fig. 7D). Similarly, no difference was observed in food or energy intake (Fig. 7, E and F). GTT and insulin tolerance test (ITT) analysis revealed no significant differences (Fig. 7, G and H), implying that the expression of the *CIDEA* mutant transgene in mouse adipose tissue does not induce any metabolic alterations. Indirect calorimetry to analyze consumed oxygen, exhaled carbon dioxide, respiratory exchange ratio, and ambulatory activity revealed no significant difference between groups (Fig. S5). Finally, we assessed fasting serum lipids including total cholesterol, nonesterified FAs, LDL cholesterol, and HDL cholesterol. No significant differences were observed among lipid parameters between Ad-CIDEA_{mut} and floxed-controls fed regular chow or HFD (Fig. 7, I–L). In addition, there was no observable difference in size or morphology of adipocytes from either chow diet-fed or HFD-fed floxed *versus* Ad-CIDEA_{mut} mice (Fig. S6). Overall, the results revealed that the expression of mutant *CIDEA* transgene in adipose tissue of mice does not exhibit any physiological or metabolic effects. Thus, Ad-CIDEA_{mut} mouse model acted as a negative control displaying *CIDEA* (556G→T) as nonfunctional.

Discussion

Here, we provide evidence for a direct role of human *CIDEA* in regulating systemic lipid and glucose homeostasis. *CIDEA* is a key protein in maintaining lipid droplet dynamics and lipolysis in adipocytes (16, 38, 39), and there is a uniformly positive correlation between *CIDEA* expression and insulin sensitivity in humans (15, 18, 19, 25, 30, 31). Interestingly, a single nucleotide mutation in *CIDEA* that causes premature truncation is associated with profound metabolic dysfunction (19). We sought to establish the mechanistic role of human

CIDEA in lipid metabolism and whole-body glucose homeostasis. This investigation was spurred by our clinical observations that *CIDEA* plays a key role in insulin sensitivity regulation and lipolysis in human adipose tissues that are not fully explained by ATGL and HSL expression levels. We generated two mouse models expressing a single copy of full-length human *CIDEA* (Ad-CIDEA_{tg}) or the *CIDEA* truncation variant (Ad-CIDEA_{mut}) in adipose tissue. Ad-CIDEA_{tg}, but not Ad-CIDEA_{mut} mice, exhibited reduced fasting glucose levels compared to their floxed-littermate controls. Similarly, Ad-CIDEA_{tg} mice were protected against HFD-induced insulin resistance and exhibited lower circulating FFA. Our RNA-seq analysis revealed changes in lipid metabolism pathways in the adipose tissue of Ad-CIDEA_{tg} mice. Lipidomics of serum samples confirmed a decrease in every measured serum FA species in HFD-fed Ad-CIDEA_{tg} mice. Together, our findings demonstrate that *CIDEA* plays a key role in controlling lipolysis and whole-body glucose homeostasis, and mechanistic studies revealed that *CIDEA* regulates the catalytic activity of ATGL to restrict the release of FFAs by interacting with CGI-58.

Obesity-induced downregulation of *CIDEA* is more pronounced in VAT than SAT, and weight loss surgery restores *CIDEA* expression levels and improves insulin sensitivity in humans (18). Indeed, our clinical data showed that obese subjects had lower *CIDEA* expression in VAT than SAT. Surprisingly, patients with obesity displayed significantly increased visceral adipose lipolysis without any differential expression in ATGL and HSL. However, our study did not exclude the possibility of changes in HSL phosphorylation, which is required for HSL activity (40). The direct effect of *CIDEA* on lipolysis was evident when we modulated *CIDEA* expression in human adipose tissue. Recombinant *CIDEA* reversed lipolysis and restored insulin sensitivity in human VAT (30). These results confirmed the negative association of *CIDEA* expression with lipolysis and insulin resistance in human adipose tissue (15, 19, 27, 30).

Gene orthologs often, but not always, have a similar function in closely related species (41). Similarly, whole-body *CIDEA* deletion in mice and *CIDEA* mutation in humans lead to dramatically different phenotypes (19, 21, 23). Interestingly, *CIDEA* KO mice exhibit higher mitochondrial oxidation and insulin sensitivity (21, 23), but adipose tissue-specific knock-down causes hepatosteatosis and insulin resistance in HFD-fed mice (42). For this reason, we kept the endogenous mouse *CIDEA* intact in our transgenic mice models. We sought to determine the functional role of human *CIDEA* in whole body metabolism and elucidate the mechanism of action. A similar human transgene expressed in mice was used to elucidate the physiological role of the human *CIDEA* gene (43). This study showed that transgenic mice expressing human *CIDEA* in adipose tissue display improved metabolic profile through expansion of adipose tissue, complementing studies in humans (44–46).

Optimal ATGL activity must be maintained to provide FFAs to tissues as a source of energy. ATGL is a rate-limiting enzyme during lipolysis (7). Yet, its role extends beyond

CIDEC improves glucose homeostasis and whole-body metabolism

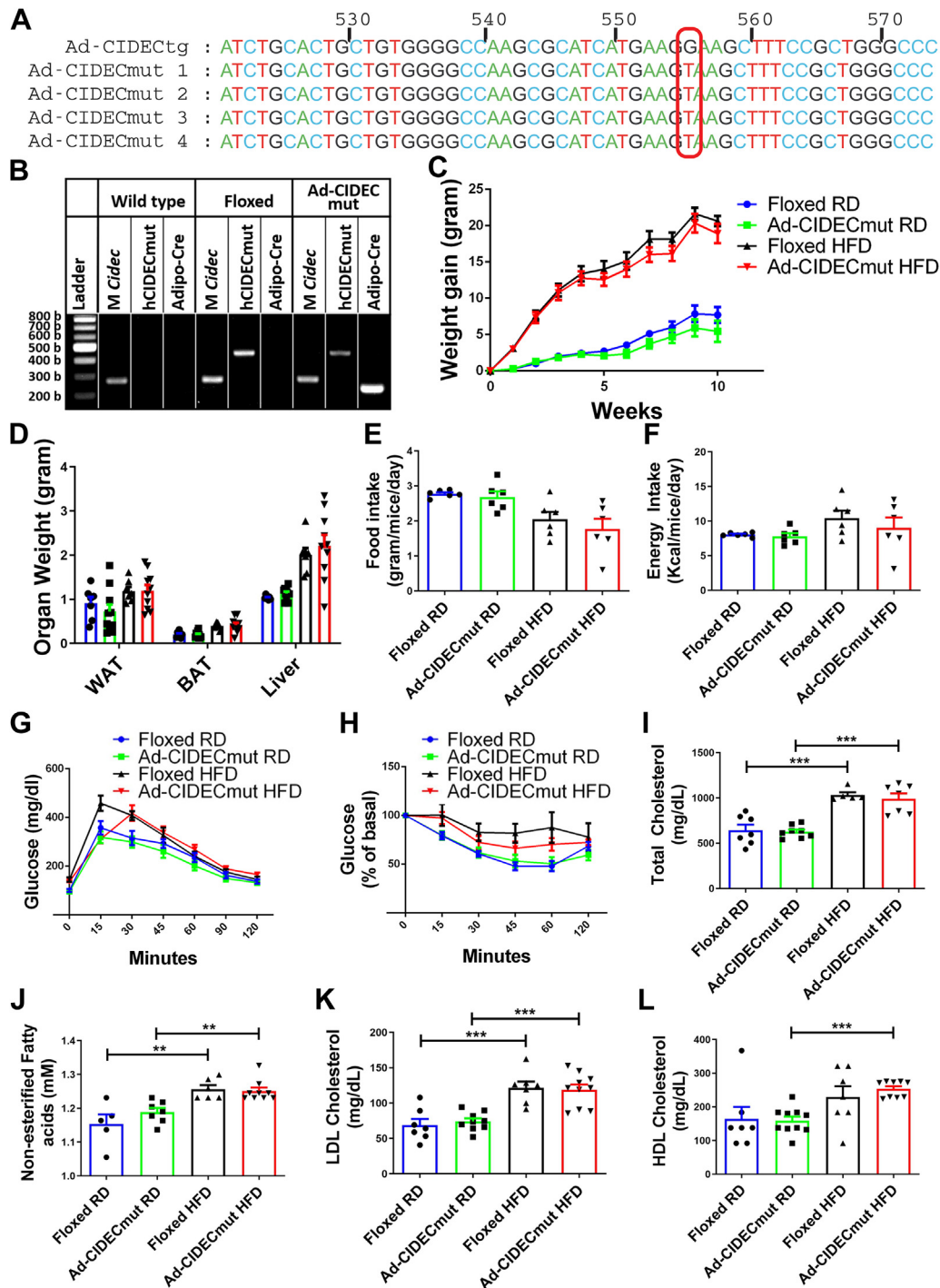


Figure 7. Generation, characterization, and metabolic studies in Ad-CIDECmut mice. *A*, DNA sequence of human *CIDEC* transgene expressed in Ad-CIDECtg mice compared to mutant *CIDEC* transgene expressed in Ad-CIDECmut mice. *B*, genotyping of Ad-CIDECmut mice for the presence of mutant *CIDEC* and/or *Cre* recombinase. M *Cidec* represents mouse *Cidec* gene. *C*, body weight gain of floxed and Ad-CIDECmut mice fed either regular chow or HFD. *D*, organ weight of floxed and Ad-CIDECmut mice. Blue, green, black, and red bars represent floxed RD, Ad-CIDECmut RD, floxed HFD, and Ad-CIDECmut HFD, respectively. *E*, food intake and (*F*) energy intake of floxed and Ad-CIDECmut mice fed either regular chow or HFD. *G*, GTT and (*H*) ITT of mice. *I-L*, fasting serum total cholesterol (*I*), nonesterified fatty acids (*J*), LDL cholesterol (*K*), and HDL cholesterol (*L*) of floxed and Ad-CIDECmut mice fed either regular chow or HFD. Data are presented as mean \pm SEM. For statistical analysis, two-way ANOVA followed by Bonferroni post hoc analysis was performed for (*G*) and (*H*). For other graphs, a student's *t* test was applied to compare the significance between the two groups. **p* < 0.05, ***p* < 0.01, ****p* < 0.001 (*n*=6–8 per group). GTT, glucose tolerance test; HFD, high-fat diet; ITT, insulin tolerance test.

adipose tissue: ATGL null mice die prematurely due to the accumulation of excess lipids in cardiomyocytes (47). However, these mice exhibited improved glucose homeostasis, which could be explained by an accumulation of lipids in

adipose tissue due to restricted lipolysis, which in turn reduces circulating FFAs and accentuates the dependency of other tissue on glucose homeostasis, leading to glucose tolerance and insulin sensitivity (47). A slight increase in adipocyte size

along with insulin sensitivity in our Ad-CIDECTg mice could mainly be attributed to the reduced circulating FFAs. Although, increase in adipocyte size has been positively correlated with insulin resistance, there is no direct evidence suggesting that adipocyte hypertrophy could alone diminish insulin responsiveness. Previous findings that large adipocytes do not directly correlate with insulin resistance support our results (48–50). Adipose-specific deletion of ATGL resulted in a similar phenotype exhibiting a marked increase in glucose and insulin sensitivity (51). Our evidence of CIDEC involvement in regulating lipid homeostasis led us to further investigate the intricate lipolytic cascade to determine the place of CIDEC in the molecular pathway. We unveiled a previously unknown role of CIDEC in inhibiting CGI-58-mediated activation of ATGL. Our results showed that CIDEC interacts with CGI-58 to inhibit its action on ATGL activity. A limitation of our study is that it could not show co-immunoprecipitation of endogenous CIDEC and CGI-58 using adipocyte samples. Perhaps the high detergent concentration used to isolate the lipid-droplet associated proteins disrupts their interaction. Our analysis of high-resolution confocal 0.2 μm thin Z-sections clearly showed the close proximity of CIDEC and CGI-58, and the coimmunoprecipitation using HEK cells showed their interaction. It is yet not clear if the CIDEC and CGI-58 binding is direct or indirect. The consequences of functional interaction of these proteins were confirmed by the ATGL activity assay where CIDEC inhibited the action of CGI-58 on ATGL-mediated lipolysis. Further studies are required to identify the role of CIDEC in exercise and fasting-mediated increase in lipolysis because both physiological conditions have common pathophysiology of increased lipolysis required to maintain energy levels in the body *via* the supply of FFAs.

We hypothesized that the expression of the human 556G \rightarrow T variant in the adipose tissue of mouse would have a dominant negative effect on lipolysis and insulin resistance since CIDEC undergoes homodimeric or heterodimeric functional interactions (36). However, there was no difference in the metabolic phenotype of floxed-controls and Ad-CIDECmut mice, showing that the mutation (556G \rightarrow T) rendered CIDEC nonfunctional. This truncation is in the C terminus of CIDEC, which we earlier identified to be the most active region in regulating lipid droplet dynamics (38), TG breakdown, and in protecting adipocytes against FFA-mediated insulin resistance (16, 38). Ad-CIDECmut mice did not show protection from increased serum lipids or impaired glucose and insulin tolerance, further confirming the physiological role of full-length CIDEC in regulating glucose and lipid homeostasis.

In conclusion, our findings support a novel mechanism by which CIDEC maintains adipose tissue homeostasis by regulating the lipolytic activity of the rate-limiting enzyme ATGL, thus reducing HFD-induced lipotoxicity and glucose intolerance. This mechanism also explains why a decrease in CIDEC, as observed in the obese state or patients with CIDEC SNPs, could result in FFA flux, leading to insulin resistance and related metabolic derangements. Indeed, *ex vivo* recombinant CIDEC decreased FFA release and restored insulin signaling in adipose tissue of obese humans (30).

Furthermore, our recent study showed that FSP27-knockout (Cidec-knockout) mice presumed to be metabolically healthy based on glucose utilization and oxidative metabolism are unhealthy in terms of exercise capacity and muscular performance (52). Overall, these studies suggest CIDEC as a potential ‘drug’ or a ‘druggable’ target to reverse obesity-induced lipotoxicity and glucose intolerance.

Experimental procedures

Selection criteria of human subjects

Consecutive subjects, both men and women, with long-standing obesity (body mass index ≥ 35 kg/m², age ≥ 18 years), enrolled in the Boston Medical Center Bariatric Surgery Program, were recruited into the study. Subjects with unstable medical conditions or pregnancy were not eligible for bariatric surgery and thus excluded. The study was approved by the Boston University Medical Center Institutional Review Board. Written consent was obtained from all participants.

Collection of human tissue

Adipose tissue samples were collected intraoperatively from two separate regions. Samples of subcutaneous and visceral adipose tissue were collected intraoperatively from the lower abdominal wall and greater omentum, respectively, during planned bariatric surgery, as previously described (53, 54). Each subject provided one biopsy specimen from the subcutaneous and visceral fat depot. All biopsies were performed under fasting conditions.

Western immunoblot analysis of human samples

Protein was extracted from adipose tissue by homogenization. Ice-cold 1X lysis buffer (Cell Signaling) supplemented with protease inhibitor cocktail and phosphatase inhibitor II and III (Sigma–Aldrich). All samples were assayed for protein content using Bradford’s method. Thirty-five micrograms of total protein was subjected to electrophoresis in SDS-polyacrylamide gel under reducing conditions and blotted to a nitrocellulose membrane using the Bio-Rad Transblot Turbo Transfer system. The membranes were blocked in Tris-buffered saline (TBS) with 0.1% Tween-20 and 5% bovine serum albumin (BSA) for 1 h at room temperature (RT) and then incubated overnight with primary antihuman antibodies against respective proteins (1:500–1000 dilution) at 4 °C. Membranes were then washed off using TBS and incubated with horseradish peroxidase (HRP)-conjugated secondary anti-rabbit IgG (R&D System) for 1 h at RT. Immune complexes were detected with the enhanced chemiluminescence ECL detection system (Bio-Rad). Densitometric analysis of bands was performed using the ImageQuant LAS 4000 bio-molecular imaging system (GE Healthcare). GAPDH was used as a loading control to normalize the quantification.

Lipolysis assessment of human adipose tissue samples

The subcutaneous and visceral fat (0.5–1 g) were cut into 1 to 2 cm explants, washed, and incubated in Phenol-Red free

CIDEc improves glucose homeostasis and whole-body metabolism

Dulbecco's modified Eagle's medium (DMEM) with 2% FA-free BSA for 2 h at 37 °C at basal conditions. At the end of the experiment, media was collected, and glycerol content in the media was measured colorimetrically at 540 nm using the Glycerol Cell-Based Assay Kit (Cayman Chemical) against a set of glycerol standards. Tissue from each experiment was collected and homogenized to measure total protein content as described in the Western immunoblot analysis before. Data were calculated as nanomole of glycerol.

Gene expression in human samples

Fragments of subcutaneous and visceral human adipose tissue were collected in RNAlater solution (Sigma–Aldrich) and stored at –80 °C. Samples were homogenized, and total RNA was isolated using RNeasy Mini kits (Qiagen). The RNA (0.5–1 µg) was retrotranscribed with high-capacity cDNA Synthesis Kits (Applied Biosystems). Quantitative real-time PCR reactions were performed using TaqMan gene expression assays in a ViiA7 PCR system (Applied Biosystems). Results were analyzed with the $\Delta\Delta C_t$ method using GAPDH as a reference.

Generation of Ad-CIDEcTg mice

Transgenic mice lines were generated using Rosa26 knock-in system. The human CIDEc gene was cloned in ROSA26-CMV-loxSTOPllox vector, and mice were generated according to the standard approach by ES cells (55). Generated mice were bred with WT C57BL/6 mice for the next (six) generations and monitored for the presence of human CIDEc transgene using standard genotyping method with human CIDEc-specific primer pairs as described later. The transgenic-floxed mice positive for human CIDEc transgene were selected and crossed with the mice containing Cre-recombinase under adiponectin promoter (B6.FVB-Tg (Adipoq-cre)1Evdrr/J mice purchased from Jackson Laboratory) to express human CIDEc specifically in adipocytes (Ad-CIDEcTg mice). The mice were maintained on a regular chow diet for 3 months. At 3 months of age, both floxed-controls and Ad-CIDEcTg mice were shifted to either a standard chow diet (10% calories from fat) or a HFD (60% calories from fat) for the next 10 weeks. Body weight was monitored weekly. At the end of the experiment, mice were fasted overnight, either pulsed or not pulsed with insulin (0.75 IU/kg of body weight), and blood and organs were collected. Serum was isolated from the blood by centrifugation, and organs were processed as per the specific analysis. IACUC approved all the protocols at the OHIO University, Athens, OH.

Genomic DNA isolation and genotyping

Genomic DNA was isolated from the mice's ear punch using the NaOH method. Briefly, ear samples were collected in 1.5 ml microcentrifuge tube, to which 50 µl of NaOH-EDTA solution (25 mM NaOH, 0.2 mM EDTA) was added. The microcentrifuge tube was then heated at 100 °C for 1 h. Samples were centrifuged briefly, and 50 µl Tris–HCl solution (40 mM Tris–HCl, pH 5.0) was added. Samples were vortexed briefly and used for amplification of specific sequences.

GTT and ITT

For the analysis of glucose homeostasis, the GTT and the ITT were performed. For GTT, mice were fasted overnight. After fasting, 1.5 g/kg of glucose was injected intraperitoneally. Blood glucose was monitored at different time points from 0 to 120 min using GE100 blood glucose monitoring system glucometer (GE Healthcare). For ITT, mice were fasted for 6 h. After fasting, 0.75 IU/kg insulin (Sigma–Aldrich) was then injected intraperitoneally. Blood glucose was monitored at different time points from 0 to 120 min. GE100 blood glucose monitoring system glucometer (GE Healthcare) was used to measure blood glucose concentrations.

Body composition analysis

For the analysis of body fat distribution, mice were placed in a whole body composition analyzer (Bruker minispec live mice analyzer, LF50). Whole body fat mass and whole body lean mass data were collected and normalized with the total body weight of mice.

Metabolic profiling of mice

To assess the changes in metabolic rate and energy expenditure, mice were placed in the Comprehensive Lab Animal Monitoring System (CLAMS) (Columbus Instruments). Mice were acclimatized for the initial 2 days in CLAMS. The changes in the rate of VO₂, VCO₂, food intake, and movements were recorded for the next 2 days. Mice were then fasted overnight to assess changes in the metabolic parameters during fasting. Data were recorded and was analyzed using the CalR web tool (56).

Glycerol release estimation

Adipose tissue from animals was freshly isolated. Small tissue explants were washed three times with PBS and kept in DMEM media supplemented with 10% fetal bovine serum at 37 °C for 2 h. Tissue samples were then either treated with vehicle (water) or were stimulated with 2 µM of CL-316243 for the next 2 h to induce lipolysis in a serum-free medium. Subsequently, media were collected, and glycerol was estimated using free glycerol reagent (Sigma–Aldrich, catalog no.: F6428).

RNA isolation and quantitative real-time PCR analysis

Quantitative real-time PCR analysis was performed to assess relative gene expression as described earlier (57). For RNA extraction, tissue samples stored at –80 °C in TRIzol (Invitrogen) were thawed and homogenized using a bead beater. RNA was isolated using the manufacturer's instructions. Five hundred nanograms of RNA was used to prepare cDNA using the RevertAid first-strand cDNA synthesis kit (Thermo Fisher). Quantitative real-time PCR was performed using the cDNA, gene-specific primer pairs, and SYBR Green master mix (Thermo Scientific).

Western blotting

As described previously (58), adipose tissue was homogenized using bead beater in mammalian cell lysis buffer (G Biosciences) supplemented with protease and phosphatase inhibitors. Samples were centrifuged twice to isolate the clear protein fraction. An equal amount of protein (μg) was used to prepare SDS-PAGE samples. After adding the loading dye, samples were resolved on SDS-PAGE and subsequently transferred to the polyvinylidene difluoride membrane. The membrane was then blocked and probed with primary overnight followed by washing three times with TBS with Tween-20 buffer and secondary antibodies (diluted in 4% BSA in TBS with Tween-20) for the next 2 hrs. Finally, the blots were developed using HRP substrate (Immobilon Western Chemiluminescent HRP substrate, Millipore) and visualized under chemiluminescence, and images were captured using BioRad Imager.

Leptin and adiponectin ELISA

Leptin (DY498) and adiponectin (DY1119) ELISA kits from R&D Biosystems were used to measure serum concentrations of leptin and adiponectin, respectively, following manufacturer's instructions. As discussed previously (59), a 96-well plate was overnight coated with capture antibody 100 μl /well of 2 $\mu\text{g}/\text{ml}$ concentration. The wells were washed with PBS with Tween-20 (PBST) and then blocked with 1% BSA in PBST for the next 1 h. Again, wells were washed with PBST, and 100 μl of the sample (for leptin, serum was diluted 10 times, and for adiponectin, serum was diluted 100 times) was added in each well along with the standard. Post 2 h incubation, wells were washed with PBST, and 100 μl of detection antibody was added to the wells (for leptin 200 ng/ml and adiponectin 25 ng/ml). After 2 h, wells were washed, and 100 μl of Streptavidin-HRP was added for 20 min. Wells were washed with PBST, and 100 μl of substrate solution was added for the next 20 min followed by the addition of 50 μl of stop solution (2N H_2SO_4). The absorbance was determined using a spectrophotometer at 450 nm.

Total cholesterol quantification

Total cholesterol was assessed in serum samples of fasted mice using cholesterol kit from Randox laboratories (CH200) as per the manufacturer's protocol. Briefly, 5 μl of serum or standard was taken in a 96-well plate. One-hundred fifty microliters of Reagent I was added to each well keeping one well for blank control. The reaction mixture was incubated at 37 °C for 5 min followed by measurement of absorbance at 500 nm. Data were collected and absorbance values were converted to actual concentration by plotting against a standard curve.

Assessment of serum TGs

As described earlier (60), serum TGs were estimated using a TG estimation kit (TR210) from Randox laboratories as per the manufacturer's protocol. Briefly, 5 μl of serum sample or standard was taken in a 96-well plate. Two-hundred

microliters of Reagent R1 was added and the reaction was incubated at 37 °C for 10 min keeping one well as blank control. Postincubation absorbance was measured by spectrophotometer at 500 nm. Data were collected and absorbance values were converted to actual concentration by plotting against a standard curve.

HDL and LDL estimation

HDL and LDL were estimated using kits (CH8311, CH8032) purchased from Randox laboratories as per manufacturer's protocol. Briefly, 3 μl of serum sample or standard was used in a 96-well plate. About 90 μl of Reagent 1 was added to each well and the reaction was incubated at 37 °C for 5 min. It was followed by the addition of 30 μl of Reagent 2. The absorbance was read at 600 nm first after 30 s (A1) and then after 150 s for HDL and 300 s for LDL (A2). Actual absorbance was calculated by A2-A1. Absolute values were obtained by plotting against a standard curve.

Adipose tissue imaging

Explants of fresh adipose tissue were washed with PBS and fixed in 1 ml of 4% paraformaldehyde in PBS for 1 h at RT. The explants were then washed thrice with PBS, followed by staining with wheat germ agglutinin Alexa Fluor633 (5.0 $\mu\text{g}/\text{ml}$: for membrane staining) for 30 min and 4',6-diamidino-2-phenylindole (for nuclear staining) for 10 min. The tissue explants were then washed once and mounted on slides to observe under Nikon A1R confocal microscope.

HEK-293 cell culture and transfection

HEK-293 cells were cultured in complete DMEM media (with 10% fetal bovine serum, 100 units/ml penicillin, and 0.1 mg/ml streptomycin). About 2×10^5 cells/well were plated in 6-well plates. After the cells reached 70% confluency, they were transfected with plasmids for pCMV3-cMyc-ATGL (Sino biological), p-mcherryC1-CGI-58-FLAG (cloned manually), or p-mcherryC1-CIDEC-HA (cloned manually) using lipofectamine 2000 (Invitrogen). Manufacturers' protocol was exactly followed for transfection. Post 36 h, cell lysate was collected, freeze-thawed, and the whole cell lysate was used to perform an ATGL activity assay.

Cloning mouse CGI-58

Mouse CGI-58 was PCR amplified using cDNA from 3T3-L1 adipocytes. High fidelity polymerase from Takara (catalog no.: #R045) was used at the following PCR conditions to amplify mouse CGI-58 with a 2 \times FLAG tag at the C terminus. PCR conditions are as follows: initial denaturation at 95 °C for 1 min, subsequent denaturation at 98 °C for 7 s, annealing at 58 °C for 15 s, and extension at 72 °C for 40 s for a total number of 35 cycles using primers, (forward CGAGCTC AAGCTTATGAAAGCGATGGCGGCGGAGGAGG and reverse ACGCGGATCCTCACTTGTCTCATCGTCTTTG TAGTCCTTGTCTCATCGTCTTTGTAGTC). PCR product was double digested with Hind-III and Bam-H1 and gel purified. The pEGFP-N1 plasmid obtained from Addgene

CIDEC improves glucose homeostasis and whole-body metabolism

(catalog no.: #54767) was also double digested with Hind-III and Bam-HI and gel purified. A purified PCR fragment was inserted into the HindIII–BamHI digested plasmid and the positive clones were selected on kanamycin. Gene expression was confirmed by Western blotting using an anti-FLAG antibody as well as the anti-CGI-58 antibody from Santa Cruz Biotech. A single band at the expected size of ~45 kDa was observed using both antibodies, confirming robust protein expression.

ATGL activity assay

ATGL activity assay was performed as described earlier (9). Briefly, ATGL (Sino Biological, catalog no.: MG52782-CM), CGI-58-FLAG (cloning as described earlier), or CIDEC-FLAG (Sino Biological, catalog no.: HG11420-NF) were transfected into HEK-293 cells. The cell lysates were purified by centrifugation, quantified, and used in the ATGL activity assay. The assay was performed by addition of either alone or combination of 80 µg ATGL, 40 µg CGI-58, and/or 40 µg CIDEC. The final volume of ATGL activity buffer (250 mM sucrose, 1 mM EDTA, 1 mM DTT, protease inhibitor, a phosphatase inhibitor, 0.005 % BSA; pH 7.0) was 90 µl. Ten microliters of 10 mM glyceryl trilinoleate (final concentration 1 mM) was added to the aforementioned ATGL activity buffer. The complete reaction mixture (total 100 µl) volume was incubated for 30 min at 37 °C. For each measurement, 20 µl of the reaction mixture was used to assess glycerol using free glycerol reagent (Sigma).

RNA-seq analysis

Visceral adipose tissue from six animals in each group were used, and the RNA samples were pooled in two sets of three animals each, making up to two sets of pooled samples in floxed and two sets of pooled samples in the Ad-hFSP27tg group. Total RNA was extracted from the tissues of biological replicates using Trizol reagent (Life Technologies Inc). Subsequently, the total RNA was treated with DNaseI (Qiagen) to remove coisolated genomic DNA and purified using RNeasy MinElute Cleanup Kit (Qiagen). The total RNA's quality and quantity were analyzed using Agilent 2100 Bioanalyzer and Qubit 4 Fluorometer (Invitrogen), respectively. The RNA-seq libraries were prepared using NEBNext Ultra II RNA Library Prep Kit according to the manufacturer's protocol (NEB). The mRNAs were enriched using Oligo (dT) beads, and subsequently, they were fragmented into shorter fragments using fragmentation buffer. The first-strand cDNA was synthesized from the fragmented mRNA using random hexamer primers and later converted into double-strand cDNA. The resulted double-strand cDNAs were end-repaired and added with Illumina sequencing adapters. The adapter-ligated libraries were amplified using sequencing primers for the enrichment. The library's quality and insert size were determined using a bioanalyzer (Invitrogen), and the library was quantified using a Qubit fluorometer (Invitrogen). The library was diluted to 4 nM concentration and sequenced using Illumina's NextSeq 500 platform with paired-end sequencing chemistry. The resulted image files in the BCL

format were converted to FASTQ with 2 × 75 bp reads using the bcl2fastq tool (Illumina). The sequencing adapters and the low-quality reads (Phred score QV <30) were removed using a read trimming tool Trimmomatic (61). The quality-filtered reads were mapped to the mouse (strain C57BL/6J) reference genome (https://www.ncbi.nlm.nih.gov/assembly/GCF_000001635.20/) using STAR RNA-seq aligner (62) to generate BAM alignment. The read count table was generated from the BAM alignment file and general feature format of genome annotation using the HTSeq R package (63). The DEGs among different experimental pairwise combinations were identified using the edgeR package (64). The DEGs were filtered based on the minimum log₂FoldChange of 1 and false discovery rate of 0.05. Gene Annotation, GO Enrichment analyses were performed using Omicsbox (<https://www.biobam.com/omicsbox/>) and the MGI database (<http://www.informatics.jax.org/>). Gene Network analysis was done using Cytoscape (<https://cytoscape.org/>) and STRING database (<https://string-db.org/>). Pathway mapping was performed using KOBAS (65) and the KEGG database.

Confocal microscopy

Confocal microscopy was performed on Nikon A1R (Nikon) confocal microscope using 60 × oil immersion objective. Images were processed using Nikon software.

Statistical analysis

Data were expressed in mean ± SEM, unless otherwise mentioned. For statistical significance, student's *t* test was used to assess the significance between the two groups. One-way or two-way ANOVA was used to analyze significance between multiple groups followed by specific post hoc analysis as depicted in figure legends. *p* values of **p* < 0.05, ***p* < 0.01, ****p* < 0.001 were used to determine statistical significance. Data were analyzed by GraphPad Prism (version 5.01, GraphPad Software Inc).

Antibodies list

For human studies

CIDEC: Rabbit (1:1000), Thermofisher (PA5-30793), (species: Human)

ATGL: Rabbit (1:1000), Thermofisher (PA1-16974), (species: Human, Mouse)

HSL: Rabbit (1:1000) Abcam (ab45422), (species: Human)

For mouse studies

FSP27: Rabbit (1:1000) Abcam (ab198204), (species: Human, Mouse)

β-Tubulin: Rabbit (1:1000) Cell Signaling Technology (CST-2146), (species: Human, Mouse)

phospho-AKT (Ser473): Rabbit (1:1000) Cell Signaling Technology (CST-9271), (species: Human, Mouse)

AKT: Rabbit (1:1000) Cell Signaling Technology (CST-9272), (species: Human, Mouse)

ATGL: Rabbit (1:1000) Cell Signaling Technology (CST-2138), (species: Human, Mouse)

CGI-58: Rabbit (1:1000) Biovision (3901-30T), (species: Human, Mouse)

Rabbit (DA1E) mAb IgG XP Isotype Control: Rabbit (1:500) Cell Signaling Technology (CST-3900), (species: All)

Anti-rabbit IgG, HRP-linked antibody: HRP-linked secondary antibody Goat (1:5000)

Cell Signaling Technology (CST-7074), (species: All)

Primers

Human CIDEC (for genotyping): TCAGCTTGACAGATCAAACGTAAC (forward); GGATGTGCCATGTGAGTCTG (reverse)

Mouse Fsp27 (for genotyping): AGCTTGGGTCCGGAGAAACAATG (forward); GTCCATCCTTGTGAGTTGGA (reverse)

Adipo Cre (for genotyping): GGATGTGCCATGTGAGTCTG (forward); CGGACAGAAGCATTTCCTCA (reverse)

Human CIDEC (for qRT-PCR): TCCAGCTGACAA GGATGGAATACG (forward); CCTCAAGACTGTAAG CCATGATGC (reverse)

Data availability

All data are included in the article.

Supporting information—The article contains supporting information.

Acknowledgments—We thank Dr Prasenjit Mitra for the helpful discussions.

Author contributions—A. G., S. K., N. G., D. K., V. M. S., V. P., and B. B. L. methodology; S. K., N. G., A. G., V. M. S., and V. P. formal analysis; A. G., S. K., N. G., B. B., M. S., S. J., S. B., T. H. M. G., S. J., S. D., H. H., V. M. S., P. N., U. K. R., and V. P. investigation; D. K. and B. B. L. resources; A. G. and V. P. writing—original draft; V. M. S. supervision.

Funding and additional information—This work was supported by NIH/NIDDK grant R01DK101711 (V. P.), R01HL140836 (N. G. and V. P.), R01DK124126 (V. P.), funds from Osteopathic Heritage Foundation's Vision 2020 to Heritage College of Osteopathic Medicine at Ohio University (V. P.), R01 NS107315 (D. K.), R01 DK108797 (D. K.), R21 HD098056 (D. K.), P30 DK046200 (D. K.). The content is solely the responsibility of the authors and does not necessarily represent the official views of the National Institutes of Health.

Conflict of interest—The authors declare that they have no conflicts of interest with the contents of this article.

Abbreviations—The abbreviations used are: BSA, bovine serum albumin; cDNA, complementary DNA; DEG, differentially expressed gene; FA, fatty acid; FFA, free fatty acid; GTT, glucose tolerance test; HDL, high-density lipoproteins; HFD, high fat diet; HRP, horseradish peroxidase; ITT, insulin tolerance test; LDL, low-density lipoprotein; PBST, PBS with Tween-20; SAT, subcutaneous

adipose tissue; TBS, Tris-buffered saline; TG, triglyceride; VAT, visceral adipose tissue.

References

- Guilherme, A., Virbasius, J. V., Puri, V., and Czech, M. P. (2008) Adipocyte dysfunctions linking obesity to insulin resistance and type 2 diabetes. *Nat. Rev. Mol. Cell Biol* **9**, 367–377
- Despres, J. P., and Lemieux, I. (2006) Abdominal obesity and metabolic syndrome. *Nature* **444**, 881–887
- Hruby, A., and Hu, F. B. (2015) The epidemiology of obesity: a big picture. *Pharmacoeconomics* **33**, 673–689
- Boden, G. (2008) Obesity and free fatty acids. *Endocrinol. Metab. Clin. North Am.* **37**, 635–646. viii–ix
- Jenkins, C. M., Mancuso, D. J., Yan, W., Sims, H. F., Gibson, B., and Gross, R. W. (2004) Identification, cloning, expression, and purification of three novel human calcium-independent phospholipase A2 family members possessing triacylglycerol lipase and acylglycerol transacylase activities. *J. Biol. Chem.* **279**, 48968–48975
- Villena, J. A., Roy, S., Sarkadi-Nagy, E., Kim, K. H., and Sul, H. S. (2004) Desnutrin, an adipocyte gene encoding a novel patatin domain-containing protein, is induced by fasting and glucocorticoids: ectopic expression of desnutrin increases triglyceride hydrolysis. *J. Biol. Chem.* **279**, 47066–47075
- Zechner, R., Zimmermann, R., Eichmann, T. O., Kohlwein, S. D., Haemmerle, G., Lass, A., et al. (2012) FAT SIGNALS—lipases and lipolysis in lipid metabolism and signaling. *Cell Metab.* **15**, 279–291
- Zimmermann, R., Strauss, J. G., Haemmerle, G., Schoiswohl, G., Birner-Gruenberger, R., Riederer, M., et al. (2004) Fat mobilization in adipose tissue is promoted by adipose triglyceride lipase. *Science* **306**, 1383–1386
- Lass, A., Zimmermann, R., Haemmerle, G., Riederer, M., Schoiswohl, G., Schweiger, M., et al. (2006) Adipose triglyceride lipase-mediated lipolysis of cellular fat stores is activated by CGI-58 and defective in Chanarin-Dorfman syndrome. *Cell Metab.* **3**, 309–319
- Granneman, J. G., Moore, H. P., Krishnamoorthy, R., and Rathod, M. (2009) Perilipin controls lipolysis by regulating the interactions of AB-hydrolase containing 5 (Abhd5) and adipose triglyceride lipase (Atgl). *J. Biol. Chem.* **284**, 34538–34544
- Subramanian, V., Rothenberg, A., Gomez, C., Cohen, A. W., Garcia, A., Bhattacharyya, S., et al. (2004) Perilipin A mediates the reversible binding of CGI-58 to lipid droplets in 3T3-L1 adipocytes. *J. Biol. Chem.* **279**, 42062–42071
- Yang, X., Lu, X., Lombes, M., Rha, G. B., Chi, Y. I., Guerin, T. M., et al. (2010) The G(0)/G(1) switch gene 2 regulates adipose lipolysis through association with adipose triglyceride lipase. *Cell Metab.* **11**, 194–205
- Miyoshi, H., Perfield, J. W., 2nd, Souza, S. C., Shen, W. J., Zhang, H. H., Stancheva, Z. S., et al. (2007) Control of adipose triglyceride lipase action by serine 517 of perilipin A globally regulates protein kinase A-stimulated lipolysis in adipocytes. *J. Biol. Chem.* **282**, 996–1002
- Puri, V., Konda, S., Ranjit, S., Aouadi, M., Chawla, A., Chouinard, M., et al. (2007) Fat-specific protein 27, a novel lipid droplet protein that enhances triglyceride storage. *J. Biol. Chem.* **282**, 34213–34218
- Puri, V., Ranjit, S., Konda, S., Nicoloso, S. M., Straubhaar, J., Chawla, A., et al. (2008) Cidea is associated with lipid droplets and insulin sensitivity in humans. *Proc. Natl. Acad. Sci. U.S.A.* **105**, 7833–7838
- Grahn, T. H., Kaur, R., Yin, J., Schweiger, M., Sharma, V. M., Lee, M. J., et al. (2014) Fat-specific protein 27 (FSP27) interacts with adipose triglyceride lipase (ATGL) to regulate lipolysis and insulin sensitivity in human adipocytes. *J. Biol. Chem.* **289**, 12029–12039
- Jash, S., Banerjee, S., Lee, M. J., Farmer, S. R., and Puri, V. (2019) CIDEA Transcriptionally regulates UCP1 for browning and thermogenesis in human fat cells. *iScience* **20**, 73–89
- Moreno-Navarrete, J. M., Ortega, F., Serrano, M., Rodriguez-Hermosa, J. I., Ricart, W., Mingrone, G., et al. (2014) CIDEC/FSP27 and PLIN1 gene expression run in parallel to mitochondrial genes in human adipose tissue, both increasing after weight loss. *Int. J. Obes. (Lond)* **38**, 865–872

CIDEA improves glucose homeostasis and whole-body metabolism

19. Rubio-Cabezas, O., Puri, V., Murano, I., Saudek, V., Semple, R. K., Dash, S., *et al.* (2009) Partial lipodystrophy and insulin resistant diabetes in a patient with a homozygous nonsense mutation in CIDEA. *EMBO Mol. Med.* **1**, 280–287
20. Singh, M., Kaur, R., Lee, M. J., Pickering, R. T., Sharma, V. M., Puri, V., *et al.* (2014) Fat-specific protein 27 inhibits lipolysis by facilitating the inhibitory effect of transcription factor Egr1 on transcription of adipose triglyceride lipase. *J. Biol. Chem.* **289**, 14481–14487
21. Toh, S. Y., Gong, J., Du, G., Li, J. Z., Yang, S., Ye, J., *et al.* (2008) Up-regulation of mitochondrial activity and acquirement of brown adipose tissue-like property in the white adipose tissue of fsp27 deficient mice. *PLoS One* **3**, e2890
22. Puri, V., Virbasius, J. V., Guilherme, A., and Czech, M. P. (2008) RNAi screens reveal novel metabolic regulators: RIP140, MAP4k4 and the lipid droplet associated fat specific protein (FSP) 27. *Acta Physiol. (Oxf)* **192**, 103–115
23. Nishino, N., Tamori, Y., Tateya, S., Kawaguchi, T., Shibakusa, T., Mizunoya, W., *et al.* (2008) FSP27 contributes to efficient energy storage in murine white adipocytes by promoting the formation of unilocular lipid droplets. *J. Clin. Invest.* **118**, 2808–2821
24. Keller, P., Petrie, J. T., De Rose, P., Gerin, I., Wright, W. S., Chiang, S. H., *et al.* (2008) Fat-specific protein 27 regulates storage of triacylglycerol. *J. Biol. Chem.* **283**, 14355–14365
25. Sharma, V. M., Vestergaard, E. T., Jessen, N., Kolind-Thomsen, P., Nellemann, B., Nielsen, T. S., *et al.* (2019) Growth hormone acts along the PPARgamma-FSP27 axis to stimulate lipolysis in human adipocytes. *Am. J. Physiol. Endocrinol. Metab.* **316**, E34–E42
26. Sharma, R., Kopchick, J. J., Puri, V., and Sharma, V. M. (2020) Effect of growth hormone on insulin signaling. *Mol. Cell Endocrinol.* **518**, 111038
27. Hjelholt, A. J., Lee, K. Y., Arlien-Soborg, M. C., Pedersen, S. B., Kopchick, J. J., Puri, V., *et al.* (2019) Temporal patterns of lipolytic regulators in adipose tissue after acute growth hormone exposure in human subjects: a randomized controlled crossover trial. *Mol. Metab.* **29**, 65–75
28. Hoyer, K. L., Hogild, M. L., List, E. O., Lee, K. Y., Kissinger, E., Sharma, R., *et al.* (2020) The acute effects of growth hormone in adipose tissue is associated with suppression of antilipolytic signals. *Physiol. Rep.* **8**, e14373
29. Tan, X., Cao, Z., Li, M., Xu, E., Wang, J., and Xiao, Y. (2016) TNF-alpha downregulates CIDEA via MEK/ERK pathway in human adipocytes. *Obesity (Silver Spring)* **24**, 1070–1080
30. Karki, S., Farb, M. G., Sharma, V. M., Jash, S., Zizza, E. J., Hess, D. T., *et al.* (2019) Fat-specific protein 27 regulation of Vascular function in human obesity. *J. Am. Heart Assoc.* **8**, e011431
31. Slayton, M., Gupta, A., Balakrishnan, B., and Puri, V. (2019) CIDE proteins in human health and disease. *Cells* **8**, 238
32. Arner, P. (1995) Differences in lipolysis between human subcutaneous and omental adipose tissues. *Ann. Med.* **27**, 435–438
33. Miyoshi, H., Perfield, J. W., 2nd, Obin, M. S., and Greenberg, A. S. (2008) Adipose triglyceride lipase regulates basal lipolysis and lipid droplet size in adipocytes. *J. Cell. Biochem.* **105**, 1430–1436
34. Zechner, R., Kienesberger, P. C., Haemmerle, G., Zimmermann, R., and Lass, A. (2009) Adipose triglyceride lipase and the lipolytic catabolism of cellular fat stores. *J. Lipid Res.* **50**, 3–21
35. Lopez-Jaramillo, P., Gomez-Arbelaiz, D., Lopez-Lopez, J., Lopez-Lopez, C., Martinez-Ortega, J., Gomez-Rodriguez, A., *et al.* (2014) The role of leptin/adiponectin ratio in metabolic syndrome and diabetes. *Horm. Mol. Biol. Clin. Investig.* **18**, 37–45
36. Liu, K., Zhou, S., Kim, J. Y., Tillison, K., Majors, D., Rearick, D., *et al.* (2009) Functional analysis of FSP27 protein regions for lipid droplet localization, caspase-dependent apoptosis, and dimerization with CIDEA. *Am. J. Physiol. Endocrinol. Metab.* **297**, E1395–E1413
37. Kim, J. Y., Liu, K., Zhou, S., Tillison, K., Wu, Y., and Smas, C. M. (2008) Assessment of fat-specific protein 27 in the adipocyte lineage suggests a dual role for FSP27 in adipocyte metabolism and cell death. *Am. J. Physiol. Endocrinol. Metab.* **294**, E654–E667
38. Jambunathan, S., Yin, J., Khan, W., Tamori, Y., and Puri, V. (2011) FSP27 promotes lipid droplet clustering and then fusion to regulate triglyceride accumulation. *PLoS One* **6**, e28614
39. Gong, J., Sun, Z., Wu, L., Xu, W., Schieber, N., Xu, D., *et al.* (2011) Fsp27 promotes lipid droplet growth by lipid exchange and transfer at lipid droplet contact sites. *J. Cell Biol.* **195**, 953–963
40. Jocken, J. W., Roepstorff, C., Goossens, G. H., van der Baan, P., van Baak, M., Saris, W. H., *et al.* (2008) Hormone-sensitive lipase serine phosphorylation and glycerol exchange across skeletal muscle in lean and obese subjects: effect of beta-adrenergic stimulation. *Diabetes* **57**, 1834–1841
41. Liao, B. Y., and Zhang, J. (2008) Null mutations in human and mouse orthologs frequently result in different phenotypes. *Proc. Natl. Acad. Sci. U.S.A.* **105**, 6987–6992
42. Tanaka, N., Takahashi, S., Matsubara, T., Jiang, C., Sakamoto, W., Chanturiya, T., *et al.* (2015) Adipocyte-specific disruption of fat-specific protein 27 causes hepatosteatosis and insulin resistance in high-fat diet-fed mice. *J. Biol. Chem.* **290**, 3092–3105
43. Abreu-Vieira, G., Fischer, A. W., Mattsson, C., de Jong, J. M., Shabalina, I. G., Ryden, M., *et al.* (2015) Cidea improves the metabolic profile through expansion of adipose tissue. *Nat. Commun.* **6**, 7433
44. Dahlman, I., Kaaman, M., Jiao, H., Kere, J., Laakso, M., and Arner, P. (2005) The CIDEA gene V115F polymorphism is associated with obesity in Swedish subjects. *Diabetes* **54**, 3032–3034
45. Wu, J., Zhang, L., Zhang, J., Dai, Y., Bian, L., Song, M., *et al.* (2013) The genetic contribution of CIDEA polymorphisms, haplotypes and loci interaction to obesity in a Han Chinese population. *Mol. Biol. Rep.* **40**, 5691–5699
46. Zhang, L., Miyaki, K., Nakayama, T., and Muramatsu, M. (2008) Cell death-inducing DNA fragmentation factor alpha-like effector A (CIDEA) gene V115F (G->T) polymorphism is associated with phenotypes of metabolic syndrome in Japanese men. *Metabolism* **57**, 502–505
47. Haemmerle, G., Moustafa, T., Woelkart, G., Buttner, S., Schmidt, A., van de Weijer, T., *et al.* (2011) ATGL-mediated fat catabolism regulates cardiac mitochondrial function via PPAR-alpha and PGC-1. *Nat. Med.* **17**, 1076–1085
48. McLaughlin, T., Sherman, A., Tsao, P., Gonzalez, O., Yee, G., Lamendola, C., *et al.* (2007) Enhanced proportion of small adipose cells in insulin-resistant vs insulin-sensitive obese individuals implicates impaired adipogenesis. *Diabetologia* **50**, 1707–1715
49. Pasarica, M., Xie, H., Hymel, D., Bray, G., Greenway, F., Ravussin, E., *et al.* (2009) Lower total adipocyte number but no evidence for small adipocyte depletion in patients with type 2 diabetes. *Diabetes Care* **32**, 900–902
50. Yang, J., Eliasson, B., Smith, U., Cushman, S. W., and Sherman, A. S. (2012) The size of large adipose cells is a predictor of insulin resistance in first-degree relatives of type 2 diabetic patients. *Obesity (Silver Spring)* **20**, 932–938
51. Schoiswohl, G., Stefanovic-Racic, M., Menke, M. N., Wills, R. C., Surlow, B. A., Basantani, M. K., *et al.* (2015) Impact of reduced ATGL-mediated adipocyte lipolysis on obesity-associated insulin resistance and Inflammation in male mice. *Endocrinology* **156**, 3610–3624
52. Slayton, M., Balakrishnan, B., Gupta, A., Jobe, S., Puri, I., Neely, S., *et al.* (2022) Fsp27 plays a crucial role in muscle performance. *Am. J. Physiol. Endocrinol. Metab.* **322**, E331–E343
53. Karki, S., Farb, M. G., Ngo, D. T., Myers, S., Puri, V., Hamburg, N. M., *et al.* (2015) Forkhead box O-1 modulation improves endothelial insulin resistance in human obesity. *Arterioscler Thromb. Vasc. Biol.* **35**, 1498–1506
54. Farb, M. G., Tiwari, S., Karki, S., Ngo, D. T., Carmine, B., Hess, D. T., *et al.* (2014) Cyclooxygenase inhibition improves endothelial vasomotor dysfunction of visceral adipose arterioles in human obesity. *Obesity (Silver Spring)* **22**, 349–355
55. Poueymirou, W. T., Auerbach, W., Frendewey, D., Hickey, J. F., Escaravage, J. M., Esau, L., *et al.* (2007) F0 generation mice fully derived from gene-targeted embryonic stem cells allowing immediate phenotypic analyses. *Nat. Biotechnol.* **25**, 91–99
56. Mina, A. I., LeClair, R. A., LeClair, K. B., Cohen, D. E., Lantier, L., and Banks, A. S. (2018) CalR: a web-based analysis tool for indirect calorimetry experiments. *Cell Metab.* **28**, 656–666.e1

57. Gupta, A., Singh, V. K., Kumar, D., Yadav, P., Kumar, S., Beg, M., *et al.* (2017) Curcumin-3,4-Dichloro Phenyl Pyrazole (CDPP) overcomes curcumin's low bioavailability, inhibits adipogenesis and ameliorates dyslipidemia by activating reverse cholesterol transport. *Metab. Clin. Exp.* **73**, 109–124
58. Gupta, A., Beg, M., Kumar, D., Shankar, K., Varshney, S., Rajan, S., *et al.* (2017) Chronic hyper-leptinemia induces insulin signaling disruption in adipocytes: implications of NOS2. *Free Radic. Biol. Med.* **112**, 93–108
59. Gupta, A., Kumar, A., Kumar, D., Singh, R., Shankar, K., Varshney, S., *et al.* (2018) Ecliptal, a promising natural lead isolated from *Eclipta alba* modulates adipocyte function and ameliorates metabolic syndrome. *Toxicol. Appl. Pharmacol.* **338**, 134–147
60. Gupta, A., Kumar, A., Kumar, D., Nandan, S., Shankar, K., Varshney, S., *et al.* (2017) Ethyl acetate fraction of *Eclipta alba*: a potential phytopharmaceutical targeting adipocyte differentiation. *Biomed. Pharmacother.* **96**, 572–583
61. Bolger, A. M., Lohse, M., and Usadel, B. (2014) Trimmomatic: a flexible trimmer for Illumina sequence data. *Bioinformatics* **30**, 2114–2120
62. Dobin, A., Davis, C. A., Schlesinger, F., Drenkow, J., Zaleski, C., Jha, S., *et al.* (2013) Star: ultrafast universal RNA-seq aligner. *Bioinformatics* **29**, 15–21
63. Anders, S., Pyl, P. T., and Huber, W. (2015) HTSeq—a Python framework to work with high-throughput sequencing data. *Bioinformatics* **31**, 166–169
64. Robinson, M. D., McCarthy, D. J., and Smyth, G. K. (2010) edgeR: a Bioconductor package for differential expression analysis of digital gene expression data. *Bioinformatics* **26**, 139–140
65. Xie, C., Mao, X., Huang, J., Ding, Y., Wu, J., Dong, S., *et al.* (2011) Kobas 2.0: a web server for annotation and identification of enriched pathways and diseases. *Nucleic Acids Res.* **39**, W316–W322